

RESEARCH ARTICLE



Small extracellular vesicles from human adipose-derived stem cells attenuate cartilage degeneration

Chang Hee Woo^{a,b}, Hark Kyun Kim^c, Gun Young Jung^c, Youn Jae Jung^{a,b}, Kyoung Soo Lee^a, Ye Eun Yun^a, Jihoon Han^c, Jeongmi Lee^c, Woo Sung Kim^a, Ji Suk Choi^b, Siyoung Yang^d, Jae Hyung Park^{b,e,f,g}, Dong-Gyu Jo^{b,c,f,g} and Yong Woo Cho^{a,b}

^aDepartment of Chemical Engineering, Hanyang University, Ansan, Korea; ^bResearch Institute, Exostemtech Inc, Ansan, Korea; ^cSchool of Pharmacy, Sungkyunkwan University, Suwon, Korea; ^dDepartment of pharmacology, Ajou University School of Medicine, Suwon, Korea; ^eSchool of Chemical Engineering, Sungkyunkwan University, Suwon, Korea; ^fSamsung Advanced Institute for Health Science and Technology, Sungkyunkwan University, Suwon, Korea; ^gBiomedical Institute for Convergence, Sungkyunkwan University, Suwon, Korea

ABSTRACT

Osteoarthritis (OA) is a chronic degenerative disease of articular cartilage that is the most common joint disease worldwide. Mesenchymal stem cells (MSCs) have been the most extensively explored for the treatment of OA. Recently, it has been demonstrated that MSC-derived extracellular vesicles (EVs) may contribute to the potential mechanisms of MSC-based therapies. In this study, we investigated the therapeutic potential of human adipose-derived stem cells EVs (hASC-EVs) in alleviating OA, along with the mechanism. EVs were isolated from the culture supernatants of hASCs by a multi-filtration system based on the tangential flow filtration (TFF) system. The isolated EVs were characterised using dynamic light scattering (DLS), transmission electron microscopy (TEM), nanoparticle tracking analysis (NTA) and flow cytometry analysis. The hASC-EVs not only promoted the proliferation and migration of human OA chondrocytes, but also maintained the chondrocyte matrix by increasing type II collagen synthesis and decreasing MMP-1, MMP-3, MMP-13 and ADAMTS-5 expression in the presence of IL-1 β *in vitro*. Intra-articular injection of hASC-EVs significantly attenuated OA progression and protected cartilage from degeneration in both the monosodium iodoacetate (MIA) rat and the surgical destabilisation of the medial meniscus (DMM) mouse models. In addition, administration of hASC-EVs inhibited the infiltration of M1 macrophages into the synovium. Overall results suggest that the hASC-EVs should be considered as a potential therapeutic approach in the treatment of OA.

ARTICLE HISTORY

Received 4 June 2019
Revised 8 January 2020
Accepted 7 February 2020

KEYWORDS

Extracellular vesicles; human adipose-derived stem cells; immune regulation; osteoarthritis

Introduction


Osteoarthritis (OA) is the most common degenerative joint disease, characterised by inflammation and catabolic processes which lead to significant joint destruction, synovial inflammation and chronic pain [1,2]. The current pharmacological treatments for OA are typically focused on pain relief and inflammation control, but these therapies cannot prevent or treat cartilage destruction in OA. Thus, the final option for patients with end-stage knee OA is total knee arthroplasty surgery [3].

The use of mesenchymal stem cell (MSC) has emerged as a promising therapeutic strategy for knee OA treatment, as they migrate to the site of injury, differentiate into the cells of an appropriate phenotype and synthesise extracellular matrix [4–6]. In addition, MSCs have immunomodulatory properties by the secretion of anti-inflammatory factors, which can

exert anti-inflammatory and anti-catabolic effects on knee OA [7–9]. Although many clinical trials investigating MSC-based therapy have demonstrated promising outcomes, there are some drawbacks, such as the technological limitation of *in vitro* expansion, the low survival rate *in vivo* and potential immunological rejection [10–12].

Recently, most studies have shown that the therapeutic potential of MSCs can be mainly attributed to their paracrine factors, particularly small extracellular vesicles (EVs) [6,13–15]. Small EVs are nanosized membrane vesicles (30–200 nm in diameter) secreted upon a fusion of endosomal multi-vesicular bodies (MVBs) with the plasma membrane [15,16]. Several groups have reported that MSC-derived EVs have biological functions similar to those of MSCs, such as repairing tissue damage, suppressing inflammatory responses and modulating the immune system [14,17–19]. In this study, we investigated

CONTACT Yong Woo Cho ✉ ywcho7@hanyang.ac.kr Department of Chemical Engineering, Hanyang University, Ansan, Korea; Dong-Gyu Jo ✉ jodg@skku.edu School of Pharmacy, Sungkyunkwan University, Suwon, Korea

 Supplemental data for this article can be accessed [here](#).

© 2020 The Author(s). Published by Informa UK Limited, trading as Taylor & Francis Group on behalf of The International Society for Extracellular Vesicles. This is an Open Access article distributed under the terms of the Creative Commons Attribution-NonCommercial License (<http://creativecommons.org/licenses/by-nc/4.0/>), which permits unrestricted non-commercial use, distribution, and reproduction in any medium, provided the original work is properly cited.

the therapeutic effects of EVs secreted from adipose-derived stem cells on cartilage regeneration using monosodium iodoacetate (MIA)-induced rat OA model and the surgical destabilisation of the medial meniscus (DMM) model of OA *in vivo* [20,21]. Human adipose-derived stem cells (hASCs) have similar potential as other stem cells as well as higher yield upon isolation and can be expanded a long time in culture before clinical use [22]. Over the past decade, hASCs have been widely used in both preclinical studies and clinical trials for various diseases, including graft-versus-host tissue [23], ischaemia [24], rheumatoid arthritis [25] and diabetes [26]. Our study demonstrated that hASC-EVs can potentially protect cartilage from degeneration, and can at least delay cartilage degeneration in all of examined OA models. In addition, we found that hASC-EVs suppressed IL-1 β up-regulated catabolic molecules and enhanced the expression of type II collagen in human OA chondrocyte.

Materials and methods

Cell culture and extracellular vesicle (EV) isolation from conditioned medium

Primary hASCs were purchased from CEFO Bio Co., Ltd (Seoul, Korea), and growth media and supplements were purchased from Life Technologies (Carlsbad, CA, USA). hASCs at passage 5-7 were maintained in growth medium (Dulbecco's Modified Eagle's Medium (DMEM) containing 10% foetal bovine serum (FBS) and 1% penicillin/streptomycin (P/S)) at 37°C in 5% CO₂, and this medium was changed every 2-3 days. After reaching 80-90% confluence, the media was changed to conditioned medium (serum-free DMEM containing 1% sodium pyruvate (S/P), 1% L-glutamine (L-Glu) and 1% P/S) for 24 h. EVs were then isolated from this conditioned medium (CM) by a multi-filtration system based on the tangential flow filtration system (TFF). Collected CM (500 mL) was centrifuged at 300 \times g for 10 min to remove cell debris. The resulting supernatant was filtered using a 0.4 μ m cell strainer and 0.22 μ m bottle top filter to eliminate micro-vesicles. To remove soluble proteins and antibiotics, the suspension was subjected to TFF with 300 kDa MWCO capsule. The suspension was continuously circulated through the membrane filter system and concentrated at 4 mL/min of operation speed. Subsequently, phosphate buffered saline (PBS) was added to the suspension, and the cycle of TFF was repeated to remove residual soluble proteins in concentrated EV solution. EVs were obtained in a final volume of approximately 10 mL. The EVs were stored in -70°C freezers until use.

Dynamic light scattering (DLS)

The sizes of EVs were measured by DLS performed with Zetasizer Nano ZS90 (Malvern, Worcestershire, UK). EVs resuspended in PBS were placed in a UV-transparent cuvette (Sarstedt AG & Co., Germany). The performed analyses were repeated at least three times, and the mean values were reported.

Nanoparticle tracking analysis (NTA)

Immediately after the isolation of EVs, the particle concentration was measured with Nanosight LM10 (Malvern Instruments Ltd., Malvern, UK). Samples were diluted in PBS to obtain a concentration within the recommended measurement range (20-30 particles/frame), corresponding to dilutions from 1:10 to 1:100 depending on the initial sample concentration. The software settings for analysis were as follows: detection threshold 3; temperature between 20 and 23°C; number of frames 30 and measurement time 30 s. The size distribution and particle concentration each represent the mean of three individual measurements.

Transmission electron microscopy

To verify the presence of intact EVs, transmission electron microscopy image analysis was performed. EVs were fixed with 0.5% glutaraldehyde solution overnight. The fixed EVs were centrifuged at 13,000 \times g for 3 min. Then the supernatant was removed. Next, the samples were dehydrated in absolute ethanol for 10 min and placed on formvar-carbon-coated copper grids (TED PELLA, Inc., Redding, CA, USA). The grids were contrasted with 1% phosphotungstic acid for 1 min and then washed several times with absolute ethanol solution. The grids were dried off completely and then examined with a JEM-2100 F field emission electron microscope (JEOL Ltd., Japan). For cryo-TEM of the EVs, the EVs were added onto the lacey carbon grid (Electron Microscopy Science, Hatfield, PA, USA). The grid was frozen in liquid nitrogen. The samples were analysed with a Tecnai F20 Twin transmission electron microscope.

Western blot analysis

Whole-cell lysates were prepared in PRO-PREPTM protein extraction solution (iNtRON Biotechnology, Inc., Korea). The protein concentration of samples was determined using the BCA protein assay. Equal amounts of

total protein were separated in a 10% SDS-PAGE and transferred to PVDF membranes (Bio-Rad, Hercules, CA, USA). The membrane with blotted protein was blocked for 2 h at room temperature with blocking buffer containing 5% BSA and incubated with primary antibodies overnight at 4°C. Then, after washing with TBS-T, the membrane was incubated for 2 h at room temperature with secondary horseradish peroxidase-conjugated goat anti-rabbit IgG. The protein bands were visualised with enhanced chemiluminescence (Thermo Fisher Scientific, Waltham, MA, USA). Primary (CD9, CD63, Alix, GM130, Calnexin and β -actin) and secondary antibodies were purchased from Abcam (Cambridge, UK).

Flow cytometry analysis

Flow cytometry analysis (FACS) of EVs was performed using a commercially available Exo-Flow capture kit (System Biosciences, CA, USA) according to the manufacturer's protocol. Briefly, isolated EVs were captured on microbead with CD9, CD63 and CD81 antibodies provided in the kit. The EV-microbead complexes were stained by Exo-FITC that features FITC conjugated to a protein which is bind EV surface protein. The EV complexes were analysed by FACS (Novocyte Flow Cytometer, ACEA Bioscience, Inc., MA, USA). Data acquisition and analysis were performed using NovoExpress software.

EV treatment of human OA chondrocyte

Human chondrocytes-osteoarthritis (HC-OA) derived from the human articular cartilage of donors with OA was purchased from Cell Applications, Inc (San Diego, CA). Chondrocytes at passage 2-4 were used for all experiments. HC-OAs were seeded onto a 24-well culture plate at 4×10^4 cells per well and cultured for 24 h in GM (growth medium; 411 K-500, Cell Applications, Inc) at 37°C under 5% CO₂. The cells were then washed with PBS and treated with recombinant human IL-1 β (5 ng/mL; R&D Systems) with or without hASC-EVs (1×10^8 , 2×10^8 particles/mL) for 72 h.

Cell proliferation and migration

Cell proliferation was evaluated by WST-8 hydrolysis using a Cell Counting Kit-8 (Dojindo Molecular Technologies, Inc.) following the manufacturer's specifications. HC-OAs were seeded onto 96-well tissue culture plates at 5000 cells per well. Plates were incubated for 24, 48 or 72 h at 37°C with 5% CO₂ in a humidified incubator. A total of 10 μ L of CCK-8 reagent was added

to each well and incubated for 3 h. Absorbance readings were then taken at 450nm using a microplate spectrophotometer (BioTek Instruments, Winooski, VT, USA). The migration of EV-treated chondrocytes was assessed using transwell chambers with 8 μ m pore filters (Corning Inc., Corning, NY, USA). Briefly, 5×10^4 cells in 100 μ L of low serum culture medium (DMEM-F12 supplemented with 0.5% FBS and 1% P/S) were seeded in the upper chamber, and EVs or vehicle control (PBS) was added to the lower chambers. Following incubation for 16 h at 37°C, non-migrating cells were removed with cotton swabs. Cells on the underside of the membrane were fixed with 4% paraformaldehyde and stained with crystal violet solution for 15 min. Stained cells that migrated through the pores to the underside of the membrane were visualised under a microscope and counted at 10 \times magnification.

Cellular uptake of EVs

The hASC-EVs were labelled with PKH67 (Sigma, St. Louis, MO, USA) according to the manufacturer's protocol. To remove free dye aggregates, the PKH-labelled EV suspension was purified with density gradient centrifugation. HC-OAs were incubated with 5×10^8 particles/mL of PKH67-labelled EVs for 12 h and then observed by confocal laser scanning microscopy (CLSM; Zeiss, Weimar, Germany) [27,28].

Quantitative real-time polymerase chain reaction (PCR)

Total RNA was isolated from human chondrocyte using the RNA-spinTM Total RNA Extraction kit (iNtRon Biotechnology Inc., Korea) according to the manufacturer's instructions. Next, the RNA was reverse transcribed using the RT² First Strand kit, then amplified with SYBR green master mix (QIAGEN, Hilden, Germany) on a Stratagene Mx3000P (Agilent Technologies, Santa Clara, CA, USA). The relative levels of gene expression were estimated with MxPro software and normalised against glyceraldehyde 3-phosphate dehydrogenase (GAPDH). All target gene primers were purchased commercially from QIAGEN.

ELISA

MMP-1, MMP-3 and MMP-13 in culture supernatant were quantified using enzyme-linked immunosorbent assays (ELISAs) according to the manufacturer's protocol (Abcam). The absorbance was measured at 450 nm using a microplate spectrophotometer.

Animals

Male Sprague-Dawley rats (7 weeks of age, 200–250 g) were purchased from Orient Bio Co. (Seoul, Korea) and male C57BL/6 mice (9 weeks of age, 20–25 g) were purchased from DBL Co., Ltd (Korea). The animals were used after 1 week of acclimatisation. The animals were housed in pairs in a temperature-controlled room (21–22°C) with a 12-h light/12-h dark cycle. All experiments were performed in accordance with Institutional Animal Care and Use Committee (IACUC) guidelines and approved by the IACUC committees of Hanyang University (HYIACUC 2016-0258A) and Sungkyunkwan University (SKKUIACUC 2018-06-13-1).

MIA-induced OA rat model

Rats were randomised and divided into two groups based on the OA model (subacute/chronic arthritis model, $n = 50$ rats per group) and further divided into four treatment groups ($n = 6$ rats per group). Monosodium iodoacetate (Sigma) was dissolved in 0.9% normal saline. With rats under anaesthesia by isoflurane inhalation, their left knee joints received a single intra-articular injection of 3 mg MIA in a volume of 50 μ L using a 30-G needle. Control rats were injected with an equivalent volume of normal saline. hASC-EVs (1×10^8 particles) were given in a 30 μ L volume per joint. PBS and hyaluronic acid (HA, 2.67×10^6 Da, Lifecore biomedical, MN, SUA, 0.3 mg) were injected under the same condition for each group. Rats in the subacute arthritis group were treated with EVs and HA once a week for 21 days before significant OA progression (1 week after OA induction). In the chronic arthritis group, treatments were given twice a week for 40 days after significant OA progression (2 weeks after OA induction). After 28 days (subacute arthritis) and 56 days (chronic arthritis) of OA induction, rats were sacrificed by CO₂ inhalation, and the knee joints of each group were dissected and the surrounding muscle was trimmed for further analyses.

Histological analysis and immunohistochemistry

The knee joints including patella and joint capsule were fixed with 10% formalin for 7 days, then decalcified with 10% EDTA solution. The decalcified specimens were embedded in paraffin, and the paraffin blocks were sagittally sectioned at 3 μ m thickness. The sections of tissue specimen were deparaffinised, dehydrated through a graded ethanol series and stained with haematoxylin

and eosin (H&E) to examine the morphology and safranin O-fast green to examine the proteoglycan deposition [29]. The stained sections were observed with a microscope (Olympus, Tokyo, Japan) and scored in terms of cartilage destruction according to the modified Mankin grading system [30]. Also, the histological changes of the infrapatellar fat pad (IFP) were assessed using histological grading protocols for synovial tissue [31]. Immunohistochemistry was performed to detect pro-inflammatory cytokine (IL-1 β) and M1 macrophages (CD86). After being deparaffinised and depleted of endogenous peroxidase activity, sections were incubated with rabbit anti-IL-1 β polyclonal antibody (1:200 dilutions, Abcam) and rabbit anti-CD86 monoclonal antibody (1:100 dilutions, Abcam) overnight at 4°C. The sections were then incubated with the respective secondary antibody, and then sections were finally stained with a diaminobenzidine (DAB) kit and counterstained with haematoxylin. For quantification analysis of IL-1 β and CD86, a total number of cells and the number of positively stained cells were evaluated, and results were expressed as the percentage of positively stained cells using three sections from each group.

Destabilisation of the medial meniscus (DMM) mouse model

The mice were anaesthetised through intra-peritoneal injection of a cocktail containing both rompun (10 mg/kg) and ketamine (40 mg/kg) and randomly distributed into experimental and control groups. DMM surgery was performed in the left knee joints following the transection of the medial meniscotibial ligament, as previously described [20]. Sham surgeries were performed with only a medial capsulotomy. EVs (1×10^8 particles) and PBS were given in a 6 μ L volume per joint. Starting from 5 weeks after DMM surgery, hASC-EVs and PBS were injected once a week. At 11 weeks post-DMM, mice were sacrificed, and their knee joints were harvested for further analyses. The degree of cartilage destruction was scored according to the OARSI histopathology system for mouse [32].

Small RNA sequencing and data analysis

RNA purification from hASC-EVs, library construction, cluster generation and sequencing was performed by Macrogen (Seoul, Korea). Briefly, hASC-EVs RNA was extracted using the Maxwell RSC miRNA from plasma (Promega, Madison, WI, USA) according to the manufacturer's instructions. The 10 ng of RNA isolated from each sample was used to construct sequencing libraries with the SMARTer smRNA-Seq

Kit for Illumina (Takara Bio, Shiga, Japan), following the manufacturer's protocol. The libraries were sequenced on an Illumina HiSeq 2500 instrument (Illumina, San Diego, California). Sequence alignment and detection of known miRNAs were performed using miRDeep2 software algorithm. miRNA target genes were predicted using publicly available algorithms including miRwalk online prediction software (<http://mirwalk.umm.uni-heidelberg.de/>) and TargetScan 7.2 (www.targetscan.org). The gene ontology (GO) terms enriched in the predicted target genes were determined using DAVID Bioinformatics. Kyoto Encyclopaedia of Genes and Genomes (KEGG) pathway analyses were performed using DIANA miRPATH v.3 (<http://diana.imis.athena-innovation.gr/DianaTools/index.php>).

Statistical analysis

Experimental results were expressed as means \pm standard deviations. The Student's two-tailed t-test, one-way and two-way ANOVA were performed using GraphPad Prism 8 software (San Diego, CA, USA). A *p* value of 0.05 or less was considered to be statistically significant.

Results

Characterisation of hASC-EVs

Following the guideline recommended by ISEV (International Society for Extracellular Vesicles), called MISEV2018 (Minimal Information for Studies of Extracellular Vesicles 2018) [33], EVs isolated from hASC-cultured media were characterised in terms of size, morphology and surface markers (Figure 1). The round spherical shape with double-layer membrane structure of the EVs was observed by classic and cryo-TEM analysis, and their mean diameter was determined to be 86.46 nm (Figures 1(a,b)). As shown in Figure 1(c,d), hASC-EVs were positive for EV markers including CD9, CD63, CD81 and Alix, whereas GM130 and Calnexin were not detected.

EV uptake and effect on human OA chondrocytes proliferation and migration

To determine whether hASC-EVs interact directly with chondrocytes, HC-OAs were incubated with 5×10^8 particles/mL of labelled EVs and EV-depleted fraction for 12 h. The labelled hASC-EVs were found mainly localised in the cytoplasm of the cell and around the nucleus (Figure 1(e)). These results implied that hASC-

EVs directly delivered into chondrocytes with their intact form.

To determine whether hASC-EVs can influence the migration of HC-OA, chondrocytes were incubated with increasing concentrations of EVs for 16 h. The results showed that hASC-EVs dose-dependently increased the chondrocyte migration towards media containing EVs (Figure 1(f,g)). In addition, we observed that treatment with hASC-EVs significantly promoted cell proliferation in a dose-dependent manner (Figure 2(a)).

hASC-EVs reduce the gene expression of catabolic molecules in human OA chondrocytes

We investigated whether hASC-EVs could modulate the catabolic and anticatabolic molecules in IL-1 β -treated human OA chondrocytes. The mRNA levels of MMP-1, MMP-3, MMP-13 and ADAMTS-5 increased in human OA chondrocytes following IL-1 β treatment and that these catabolic makers were significantly suppressed in the presence of hASC-EVs (Figure 2(b–e)). In addition, we detected the concentrations of MMP-1, MMP-3 and MMP-13 in the culture supernatants. We found that the hASC-EVs inhibited the IL-1 β -induced MMP production (Figure 2(g–i)). Besides, hASC-EVs treatment markedly increased mRNA expression of type II collagen suppressed by IL-1 β in human OA chondrocyte (Figure 2(e)). Similarly, there was a reduction of IL-1 β -induced genes involved in inflammation and cartilage degradation in primary mouse articular chondrocytes (Supplementary Figure S2).

Therapeutic efficacy of hASC-EVs in MIA-induced OA model

To evaluate the therapeutic efficacy of hASC-EVs in the early phase of OA, EVs were administered intra-articular weekly for 3 weeks, starting 1 week after MIA injection. At 4 weeks following MIA injection, the isolated knee joints were examined grossly after being stained with India-ink. The hASC-EVs treatment group showed that the area of eroded cartilage surface was significantly reduced compared to the PBS and HA treatment groups in the joint of the MIA model (Supplementary Figure S3).

As cartilage destruction is the main histological feature of OA, the effects of EVs on the morphological changes and severity of cartilage damage were evaluated using H&E and safranin O-fast green staining in the MIA-induced OA model. OA severity was scored using the modified Mankin scoring system (Supplementary Table 1). Histological evaluation revealed that the

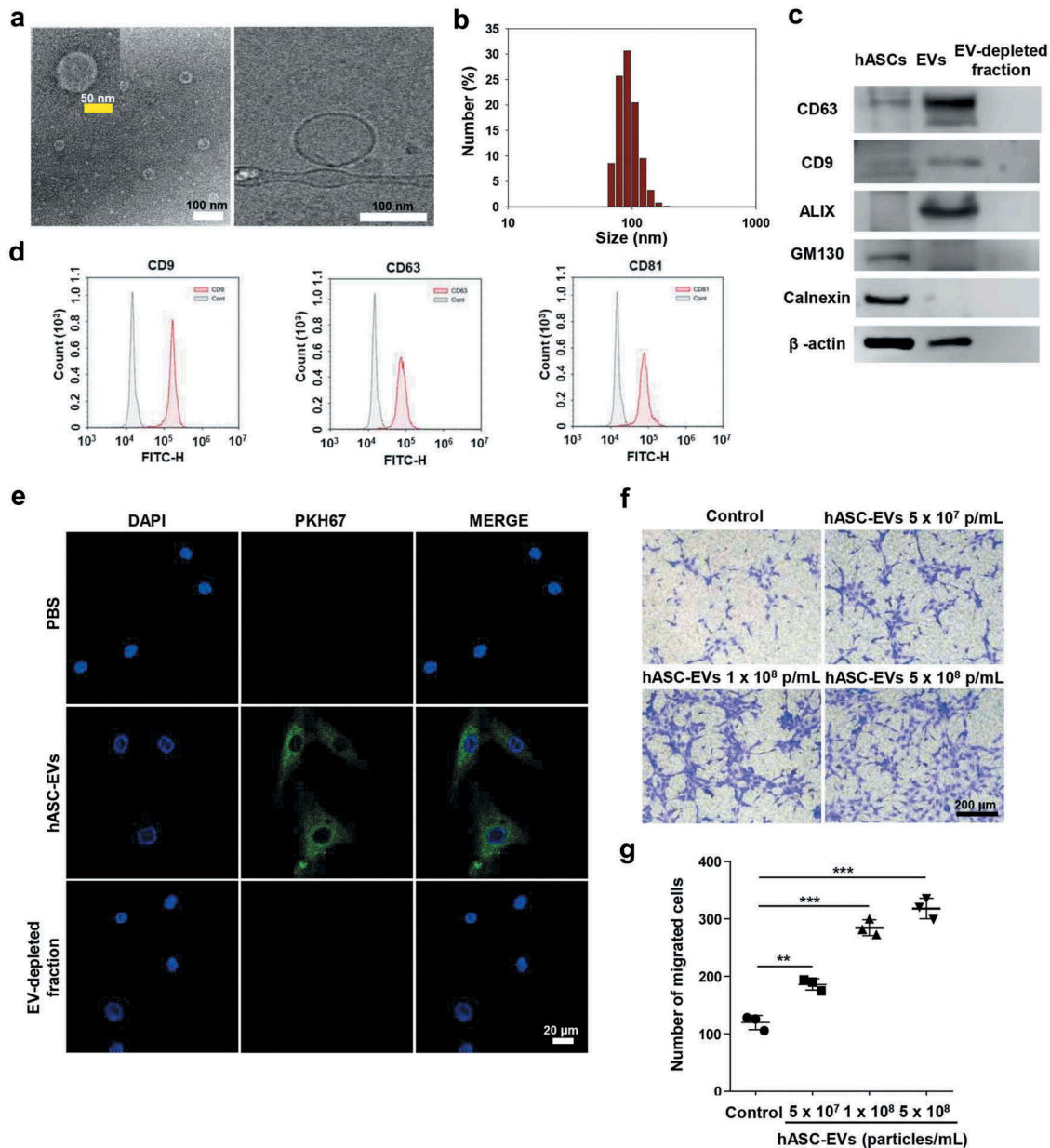


Figure 1. Characterisation of hASC-EVs. (a) Classic and cryogenic transmission electron microscope (TEM) images of hASC-EVs. (b) Dynamic light scattering (DLS) showing the particle size distribution of EVs. (c, d) EV markers (CD9, CD63, CD81, Alix) and non-EV markers (GM130, Calnexin) detection by flow cytometry and Western blot analysis. The cellular uptake and migration of hASC-EVs in human chondrocyte-osteoarthritis (HC-OA). (e) Confocal images of HC-OA after 12 h incubation with 5×10^8 p/mL of hASC-EVs. DAPI was used to stain the nuclei (blue), and hASC-EVs were labelled with PKH67 (green). Scale bars, 20 μ m. (f, g) Transwell migration assay showing the dose-dependent effect of hASC-EVs on HC-OA migration. After 16 h, the migration activity was quantified by counting the migrated cells on the underside of the membrane. Scale bars, 200 μ m. All data are shown as means \pm standard deviations of the three independent trials per treatment group. ***p* < 0.01, ****p* < 0.001.

vehicle (PBS) treatment group showed severe cartilage matrix degradation extending into the deep zone, as well as a lack of cells in the radial zone (Figure 3(a)). In the HA treatment group, the degree of cartilage damage was less than in the PBS-treated group, but a loss of chondrocyte cellularity and moderate reduction in proteoglycan content were still observed. However, when the hASC-EVs were injected, mild OA pathology appeared,

such as a slight reduction of proteoglycan and surface fissure. Therefore, the total Mankin score of the hASC-EVs treatment group was significantly lower than that of the PBS or HA treatment group (Figure 3(b)). These findings indicate that hASC-EVs treatment in this early phase of the OA model effectively prevents proteoglycan degradation and protects against the progression of cartilage destruction after MIA injection.

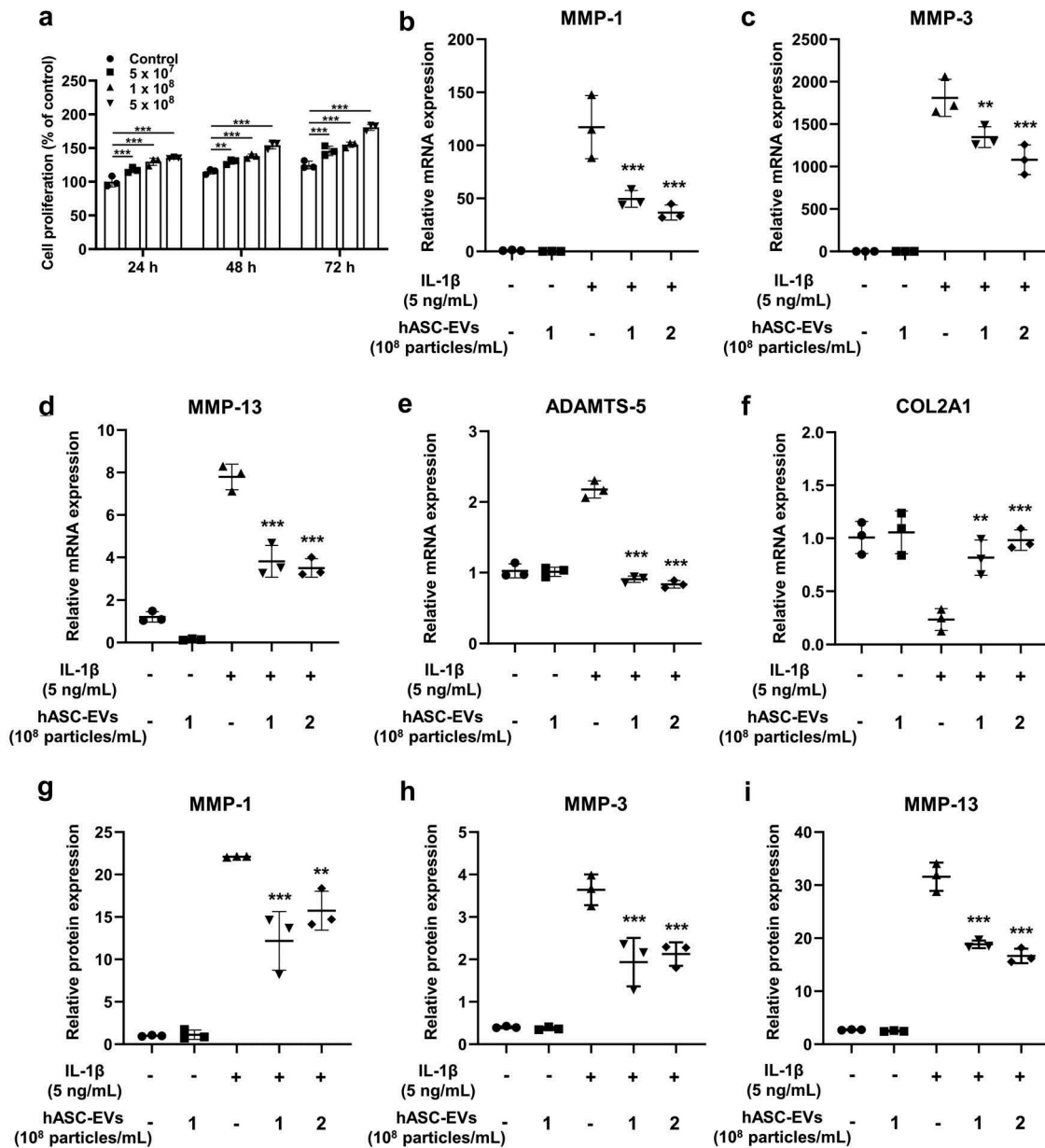


Figure 2. Effects of hASC-EVs on the mRNA levels of MMP-1, MMP-3, MMP-13, ADAMTS-5 and type II collagen in IL-1 β -treated HC-OAs. (a) CCK-8 assay showing the effect of hASC-EVs on chondrocyte proliferation at the indicated times. All data are shown as means \pm standard deviations of the three independent trials per treatment group. (b–f) HC-OAs were treated with IL-1 β (5 ng/mL) with or without hASC-EVs (1×10^8 and 2×10^8 particles/mL) for 72 h. Gene expression of catabolic and anabolic markers was determined using quantitative PCR. (g–i) Protein expression of MMP-1, MMP-3 and MMP-13 was determined using ELISA. The values were normalised to total protein concentration. All data are shown as means \pm standard deviations ($n = 3$). ** $p < 0.01$ and *** $p < 0.001$ compared to IL-1 β alone. Abbreviations: MMP, matrix metalloproteinase; ADAMTS, a disintegrin and metalloproteinase with thrombospondin motifs; COL2A1, type II collagen alpha 1.

To examine the effect of hASC-EVs in a chronic arthritis model, we injected EVs into the joint after significant OA progression. At 8 weeks after MIA injection, the histological morphologies of the PBS treatment group showed serious symptoms of OA, such as extensive loss of proteoglycan, severe fibrillation and cartilage erosion into the subchondral bone, in the whole part of the articular cartilage (Figure 3(c)). Similar histological changes were also observed in the HA treatment group,

indicating that the HA injection had no effect of cartilage protection or disease attenuation after significant OA progression. The hASC-EVs treatment group showed moderate-to-severe cartilage matrix destruction, some hypocellularity of chondrocytes and proteoglycan degradation, but these cartilage damages were significantly lower than those in the PBS or HA treatment group. The total Mankin scores of the hASC-EVs treatment group were markedly lower than those of the PBS

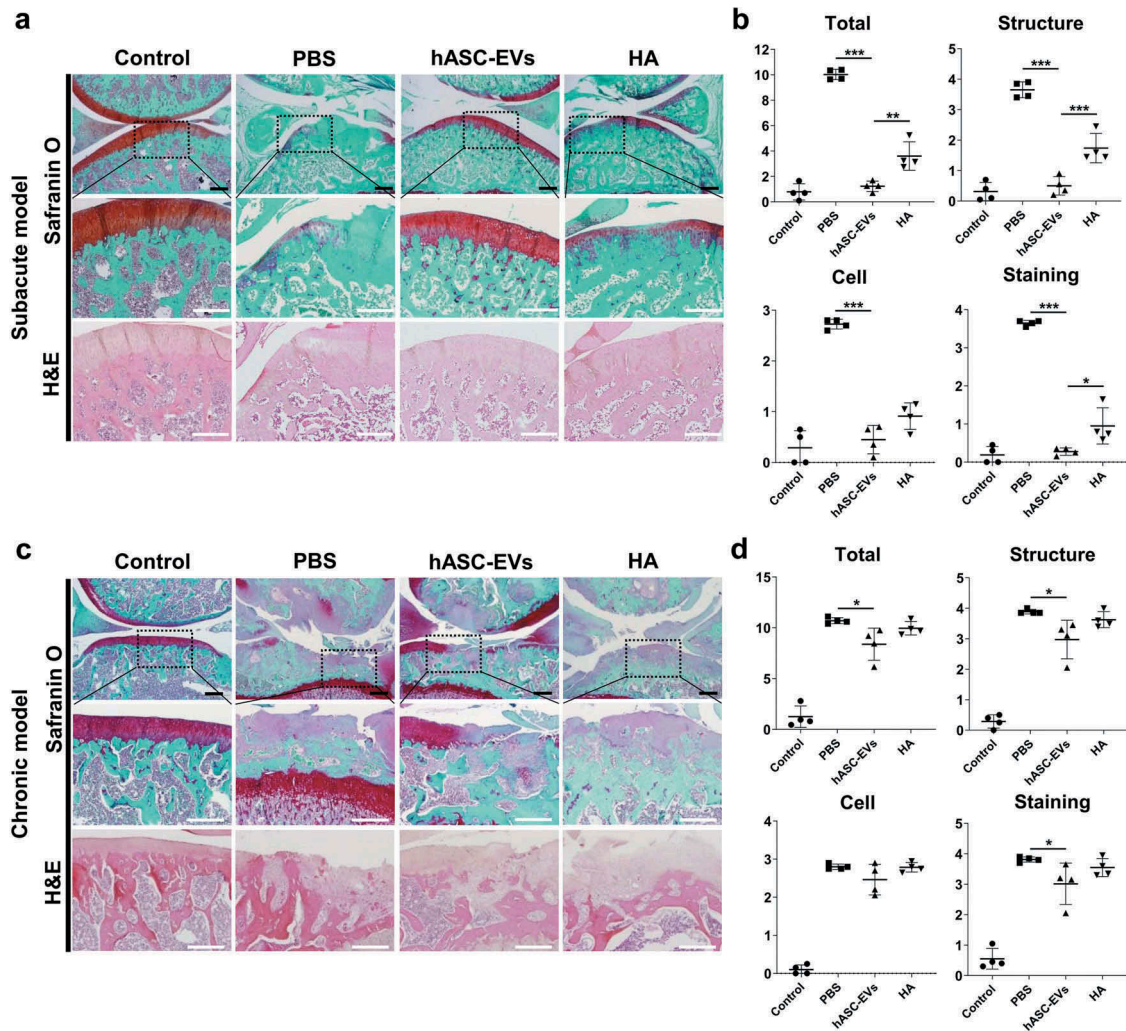


Figure 3. Effect of hASC-EVs on cartilage degradation at 4 weeks after MIA injection in a subacute arthritis model. Intra-articular injection of hASC-EVs was performed weekly, starting 1 week after MIA injection. (a) Knee joints were harvested at 4 weeks after MIA injection and analysed histologically by safranin O-fast green and haematoxylin and eosin (H&E). Black scale bars, 500 μ m. White scale bars, 400 μ m. (b) The joint lesions were graded on a scale of 0–11 using the modified Mankin scoring system, giving a combined score for cartilage structure, cellular abnormalities and matrix staining, and a total Mankin score. All data are shown as means \pm standard deviations ($n = 4$). *** $p < 0.001$. In chronic arthritis model, intra-articular injection of hASC-EVs was performed twice a week, starting 2 weeks after MIA injection. (c) Knee joints were harvested at 8 weeks after MIA injection and stained with safranin O-fast green and H&E. Black scale bars, 500 μ m. White scale bars, 400 μ m. (d) The stained sections were scored on a scale of 0–11 using the modified Mankin scoring system. All data are shown as means \pm standard deviations ($n = 4$). * $p < 0.05$.

treatment group, which is consistent with the microscopic findings (Figure 3(d)). These results suggest that hASC-EVs treatment did not completely prevent progressive joint disease or repair impaired cartilage, but did attenuate the cartilage degradation after significant OA progression.

Alleviation of OA by hASC-EVs in DMM model

We also evaluated the therapeutic effects of hASC-EVs on DMM model, which is a well accepted *in vivo* model for progressive OA (Figure 4(a)). Histological evaluation

revealed that the PBS treatment group showed the severe erosion of the calcified cartilage and extensive loss of proteoglycan (Figure 4(b)). However, the hASC-EVs treatment group showed small fibrillations and vertical clefts down to the layer immediately below the superficial layer. The OARSI grade of the hASC-EVs treatment group revealed significantly lower than that of the PBS treatment group (Figure 4(c) and Supplementary Table 2). To further examine the effect of hASC-EVs on cartilage matrix cleavage, protease activity was analysed by immunostaining for cleaved aggrecan (NITEGE). hASC-EVs treatment strongly reduced the levels of NITEGE in hASC-EVs treated DMM

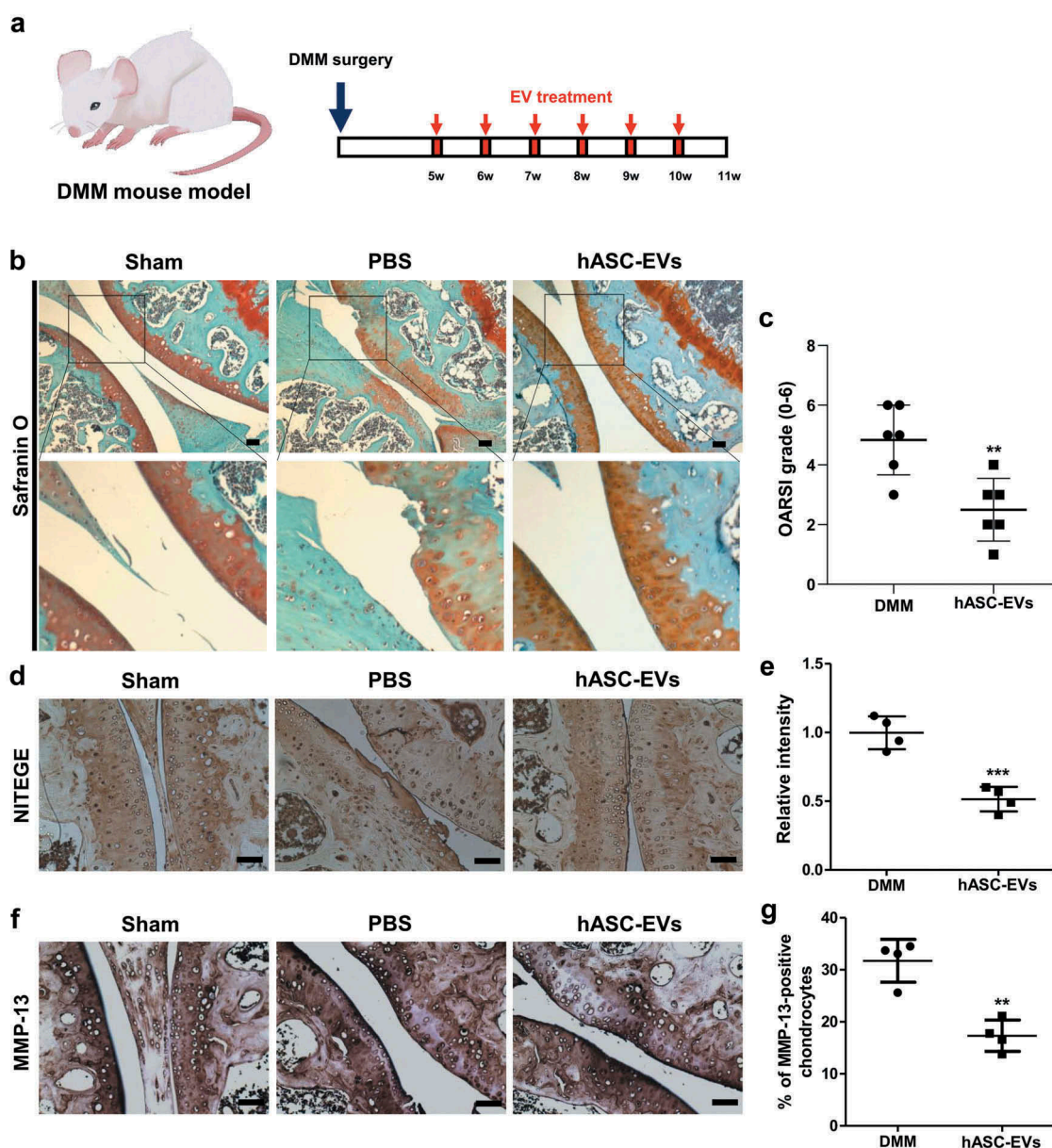


Figure 4. Effect of hASC-EVs on cartilage degradation at 11 weeks after destabilisation of the medial meniscus (DMM) surgery. Intra-articular injection of hASC-EVs was performed weekly, starting 5 weeks after DMM surgery. (a) Schematic illustration of the in vivo animal test for evaluating the efficacy of hASC-EVs on cartilage degradation in DMM mouse model. (b) Knee joint was harvested at 11 weeks after DMM surgery and analysed histologically by Safranin O-fast green. Scale bars, 100 μ m. (c) The joint lesions were graded on a scale of 0–6 using the OARSI scoring system. All data are shown as means \pm standard deviations ($n = 6$). ** $p < 0.01$. (d) Immunohistochemical staining of cleaved aggrecan (NITEGE) and (e) quantitative analysis of the relative intensity of NITEGE in the articular cartilage. (f) Collagenase 3 (MMP-13) staining and (g) quantitative analysis of the MMP-13-positive chondrocytes in the articular cartilage. Scale bars, 200 μ m. All data are shown as means \pm standard deviations ($n = 4$). ** $p < 0.01$ and *** $p < 0.001$.

mice compared to the control group (Figure 4(d,e)). DMM surgery also induces the expression of MMP-13 in articular cartilage. MMP-13 is known to cleave type II collagen and mediates cartilage matrix degradation. hASC-EVs treatment also reduced the percentage of MMP-13-positive chondrocytes in DMM mice (Figure 4(f,g)). These findings suggest that hASC-EVs treatment in DMM model of OA effectively

prevents the fibrillation and protects against the erosion of cartilage matrix after DMM surgery.

hASC-EVs attenuate cartilage matrix degradation

To explore the mechanisms underlying the attenuated degradation of the cartilage matrix in hASC-EVs treated

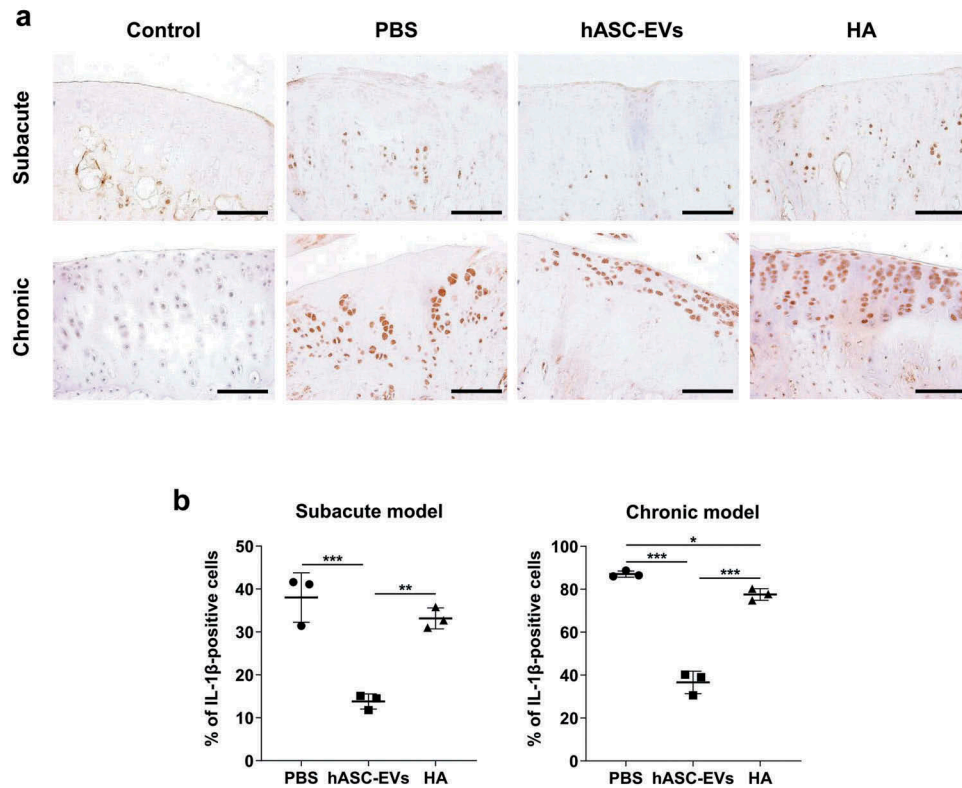


Figure 5. Effect of hASC-EVs on the expression of IL-1 β in the articular cartilage of the subacute and chronic arthritis models. (a) Immunohistochemical staining of IL-1 β and (b) quantitative analysis of the expression of IL-1 β in the articular cartilage. Scale bars, 100 μ m. All data are shown as means \pm standard deviations of three independent trials per treatment group. ** p < 0.01 and *** p < 0.001 compared to PBS group.

rats after MIA injection, we performed immunohistochemical staining to examine the expression of IL-1 β . The expression of IL-1 β , the main mediator of the induction of the cartilage degradative enzymes, was markedly increased in the MIA-induced OA model (Figure 5(a)). Immunohistochemistry staining showed that hASC-EVs treatment significantly decreased the number of IL-1 β positive cells of the subacute and chronic arthritis model by 13.8% and 36.6%, respectively, compared to the PBS treatment groups (Figure 5(b)). These findings suggest that the intra-articular injection of hASC-EVs reduces the degradation of cartilage matrix through inhibiting the expression of IL-1 β .

Effect of EVs on the synovial inflammation

MIA injection of the knee joint induced not only cartilage degradation but also changes in other joint tissues, including the perimeniscal synovium and infrapatellar fat pad (IFP). Here, we examined the effects of hASC-EVs on the inflammatory responses in perimeniscal synovium and IFP. In the subacute arthritis model, synovial inflammation including subintimal fibrosis and neovascularisation was observed in the PBS treatment groups. However, hASC-

EVs treatment essentially prevented fibrotic deposition and blood vessel formation, and also maintained the adipocyte-rich appearance of the IFP (Supplementary Figure S4A). Severe synovial inflammation, including hyperplasia, extensive subintimal fibrosis, hyper-vascularisation and fragments of cartilage, were found in the PBS groups of the chronic arthritis model, whereas hASC-EVs treatment group showed a reduced degree of synovial inflammation. To provide quantitative histopathology data of the IFP, we applied a multi-parameter scoring system (Supplementary Table 3) for cellularity, fibrosis and vascularity (Supplementary Figure S4B, C). These results suggested that the hASC-EVs treatment attenuated the inflammatory responses in synovium and fibrotic remodelling and blood vessel formation in IFP tissue, but that PBS and HA treatment were ineffective in this regard.

hASC-EVs decrease M1 macrophage infiltration and the production of pro-inflammatory cytokine (IL-1 β) in perimeniscal synovium

Since it has been reported that the inflammatory response of the synovium is strongly related to OA development, the immunity components were

examined using immunohistochemical staining [34]. Specifically, we investigated the immune regulatory capacity of hASC-EVs on M1 macrophage infiltration into the perimeniscal synovium as well as M1 macrophage-associated cytokine, IL-1 β , in the knee joint of the MIA-induced OA model. Immunohistochemistry staining showed that hASC-EVs treatment decreased the infiltration of M1 macrophage, as indicated by CD86 cells, and also reduced the expression of pro-inflammatory IL-1 β in the synovium (Figure 6).

To validate the effects of hASC-EVs on macrophages, lipopolysaccharide (LPS) and hASC-EVs were added to the cultured RAW264.7 cells. We found that the hASC-EVs inhibited the LPS-induced COX-2, IL-1 β , IL-6 and TNF- α mRNA expression (Supplementary Figure S5A-D). Furthermore, M1 macrophage markers (iNOS and IL-1 β) were significantly reduced, whereas

the M2 marker (Arg1) was increased (Supplementary Figure S5E). These results suggest that hASC-EVs effectively inhibit the production of pro-inflammatory cytokines of macrophages, and facilitate the polarization of macrophages to pro-inflammatory (M1) phenotype rather than anti-inflammatory (M2) phenotype macrophages.

miRNA profiling and bioinformatics to analyse the miRNA of hASC-EVs

EVs can modulate recipient cells through miRNA regulation of post-transcriptionally coding genes [35]. Thus, we profiled and quantified the miRNA in hASC-EVs. To profile hASC-EVs miRNA, total RNA was purified from hASC-EV and used for small RNA sequencing. The top 50 known miRNAs

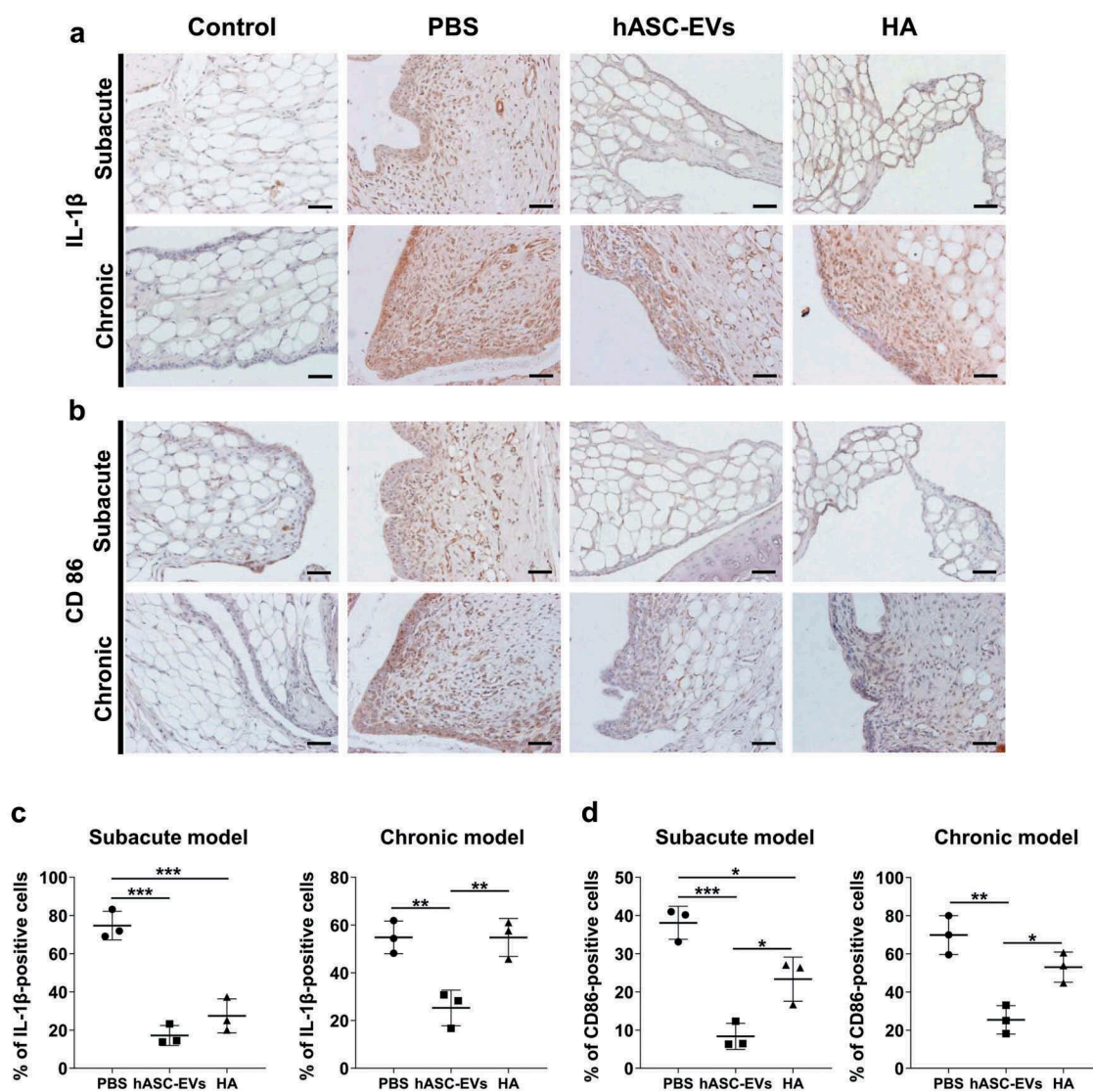


Figure 6. Immunohistochemical staining was used to identify the expression IL-1 β (a, b) and CD 86 (c, d) and quantitative analyses of IL-1 β and CD86 cells on synovium. Scale bars, 50 μ m. All data are shown as means \pm standard deviations ($n = 3$). ** $p < 0.01$ and *** $p < 0.001$.

detected in hASC-EVs were ordered according to the total read count (Figure 7(a)). Among enriched miRNAs in hASC-EVs, the expression levels of miR-199a, miR125b, miR-221 and miR-92a are previously reported to be decreased in the OA pathology [36–39]. To further investigate miRNAs, functional enrichment analyses of the top 50 known miRNAs were performed. We performed KEGG pathway analysis to identify dominant pathways controlled by hASC-EVs (Figure 7(b)). KEGG pathway enrichment indicated “ECM-receptor interaction”, and “glycosphingolipid biosynthesis – lacto and neolacto series” as enriched pathway. GO analysis revealed that, “positive regulation of transcription from RNA polymerase II promoter” in the biological process category; “nucleoplasm” and “membrane” in the cellular component category and “protein binding” and “protein serine/threonine kinase activity” in the molecular function category, were observed to be significant (Figure 7(c–f)). Collectively, these results indicate a possible contribution of miRNAs in protecting cartilage from degeneration.

Discussion

MSC-derived EVs have emerged as a prominent candidate for therapeutic application in degenerative diseases via tissue regeneration and immune regulation [13,15]. Increasing evidence has shown the beneficial effects of EV treatment on an OA animal model using human embryonic MSCs or synovium MSCs [40,41]. EVs can be considered as regulators of cell-to-cell communication to transfer lipid, nucleic acids (mRNAs and microRNAs) and cell-specific proteins between cells to elicit diverse cellular responses in recipient cells [15]. In particular, MSC-derived EVs play a crucial role in maintaining normal cellular homeostasis [42]. This role is particularly important when cartilage homeostasis is disrupted in OA with an imbalance in the catabolic and anticatabolic mediators. In the early phase of OA, catabolic activity is intensified by the increased expression of inflammatory mediators and cartilage-degrading proteinases [43]. Therefore, early therapeutic intervention is important for preventing the serious progression of OA. In this study, we demonstrated that the intra-articular injection of hASC-EVs could effectively attenuate the development of OA in the subacute and chronic arthritis models by reducing the inflammatory response.

Inflammation is considered to be a key driver of OA pathogenesis. The pro-inflammatory cytokines are significantly elevated in the synovial fluid of OA patients, and they play critical roles in the pathogenesis of OA [34,44]. Among the pro-inflammatory cytokines, IL-1 β

and tumour necrosis factor (TNF)- α seem to be most involved in the catabolic process of OA [44,45]. In particular, pro-inflammatory IL-1 β contributes to OA development by inducing catabolic and destructive processes. IL-1 β is highly overexpressed in the synovial tissue, cartilage and subchondral bone layer, and induces matrix destructive enzymes, such as interstitial collagenase (MMP-1), stromelysin-1 (MMP-3), collagenase 3 (MMP-13) and aggrecanase 2 (ADAMTS-5), in OA [45–48]. The increased expression of these degradative enzymes would shift the balance of homeostasis towards catabolic metabolism, resulting in cartilage degradation. The established mechanisms that prevent OA development mostly depend on the inhibition of cartilage degradative enzymes [47,49,50]. Therefore, it is important to modulate the inflammatory process to prevent and attenuate OA development. Several studies have demonstrated that hASCs exhibit immunosuppressive effects both *in vitro* and *in vivo*, and may play a role in the local inflammatory process in the joint through the secretion of immunomodulatory factors such as IL-4, IL-10, IL-13 and transforming growth factor β (TGF- β) [8,9,51–55]. Especially, TGF- β 1 is one of the key regulators of inflammatory response, and is also known to stimulate ECM synthesis including aggrecan, proteoglycan and type II collagen in chondrocytes. Thus, we hypothesised that EVs released from hASCs might have an immunomodulatory role in the treatment of OA because they expressed distinctive molecules, including miRNAs and proteins, that reflected both the condition and origin of the producer cells. We found these immunomodulatory factors were expressed in hASC-EVs (Supplementary Figure S1). In particular, tissue inhibitors of metalloproteinase-1 and -2 (TIMP-1 and TIMP-2), which control the MMPs activities, were highly expressed in the hASC-EVs [56]. Furthermore, hASC-EVs have several enriched miRNAs (miR-199a, miR125b, miR-221 and miR-92a), which are related to OA pathology. Especially, miR-199a regulates the expression of COX-2 which plays an important role in OA inflammation [36].

Here, we investigated the immunomodulatory effect of hASC-EVs on human OA chondrocyte under IL-1 β treatment *in vitro*. Consistent with previous studies, IL-1 β stimulated the release of several catabolic factors from chondrocytes and appeared to produce an environment similar to the synovial fluid of OA [46,57]. The hASC-EVs treatment effectively suppressed the IL-1 β -mediated expression of MMP-1, -3, -13 and ADAMTS-5, and increased the expression of type II collagen in chondrocyte. Moreover, we observed that the hASC-EVs promote cell proliferation and the migration of human OA

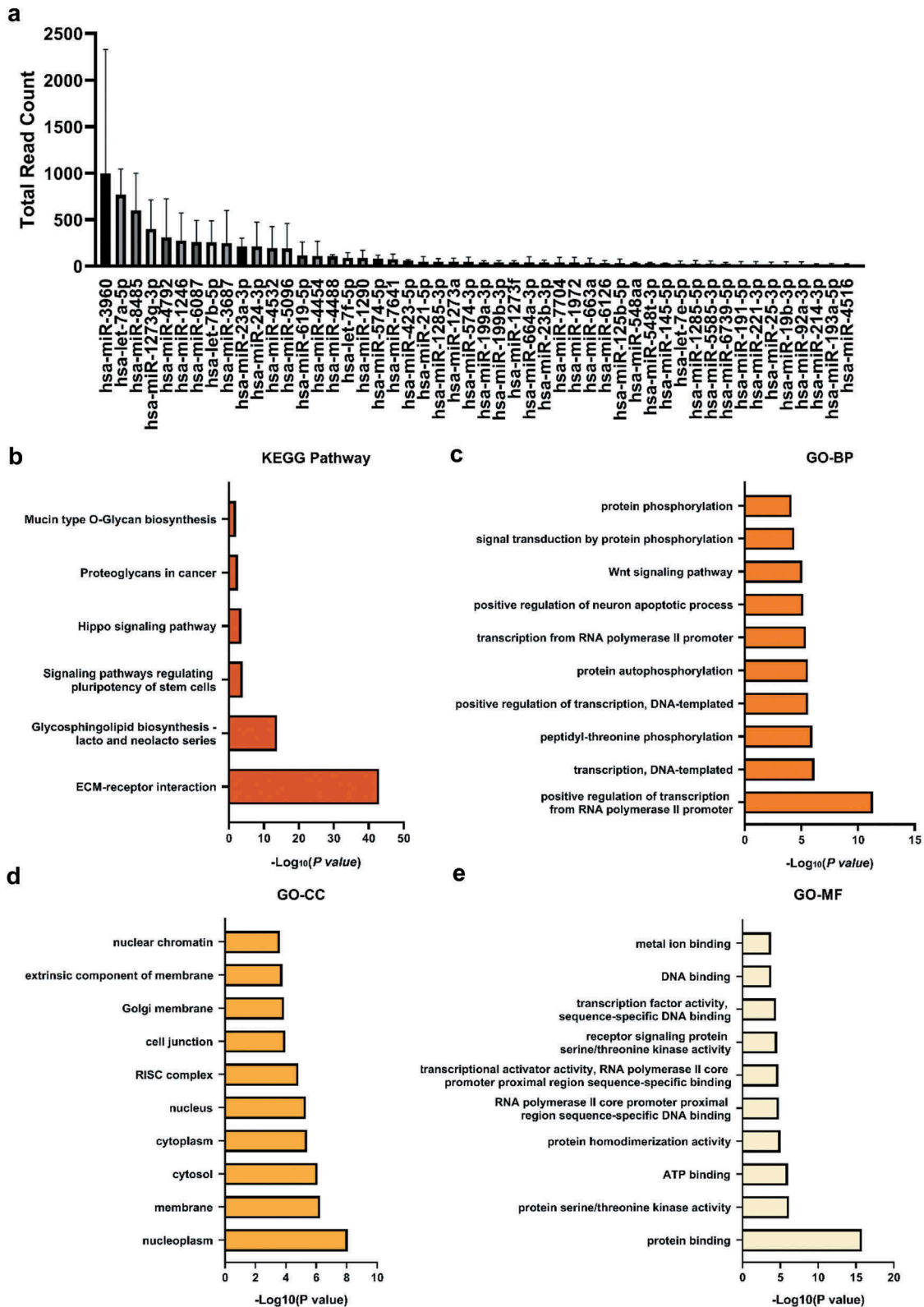


Figure 7. Next generation sequencing (NGS) of (a) top 50 known miRNAs that were detected in hASC-EVs. Total read counts are shown ($n = 2$). (b–e) KEGG and GO pathway analyses were performed on target genes of miRNAs enriched in hASC-EVs. The significantly enriched KEGG pathways and GO terms of biological processes (BP), cellular components (CC) and molecular functions (MF) were presented. Only the 10 most relevant GO terms are shown.

chondrocytes in a dose-dependent manner. The chondrocytes play a key role in the maintenance of cartilage homeostasis and the tissue repair response during the development of OA [42]. Our results suggest that the hASC-EVs treatment resulted in an increase in the proliferation and migration of chondrocyte and mediated the balance between catabolic and anabolic metabolism, leading to the recovery of the damaged cartilage.

Next, we investigated the therapeutic effect of hASC-EVs on the subacute and chronic MIA-induced OA rat models. MIA, a metabolic inhibitor, was used to induce OA changes that mimic the structural and biochemical changes associated with human OA. The protective effects of hASC-EVs were comparable to those of HA, which is a widely used therapy for OA patients by intra-articular injection [3]. In this study, we found that the hASC-EVs treatment efficiently protected articular cartilage and attenuated the development of OA in both the subacute and chronic models. In particular, the intra-articular injection of hASC-EVs in the early phase of OA exhibited substantial therapeutic effects on cartilage regeneration. This seems to be related to the enhanced expression of pro-inflammatory cytokines such as IL-1 β in the cartilage at an early stage of the MIA-induced OA model [58]. Therefore, hASC-EVs treatment in the early phase of OA could effectively modulate inflammation and promote tissue repair processes, leading to the attenuation of OA. Also, we evaluated the regenerative effect of EVs using a DMM mouse model. The surgical model of DMM has been used as a gold standard for studying the evaluation of OA progression *in vivo* by providing good reproducibility and a slower disease progression. The results also show that the EVs derived from hASCs effectively prevented the progress of cartilage destruction in an OA model.

Synovial inflammation is increasingly being recognised as an important feature of OA that can adversely affect joint function. Synovial inflammation of OA leads to synovial lining hyperplasia, fibrosis, neo-vascularisation and the appearance of macrophages [34]. Macrophages are also involved in the pathogenesis of inflammatory arthritis. Recent studies have reported that M1-polarized macrophages express numerous pro-inflammatory mediators, such as TNF- α , IL-12 and IL-1 β , and inhibit the chondrogenesis of MSC via IL-6 [59,60]. We found that hASC-EVs treatment suppressed the expression of pro-inflammatory cytokines (COX-2, IL-1 β , IL-6 and TNF- α) in RAW264.7 cells and promoted polarization of M1 to M2 macrophages. In addition, hASC-EVs inhibited the infiltration of M1 macrophages at the OA synovium, as well as the reduction of pro-inflammatory IL-1 β in both the synovium and cartilage regions in MIA-induced OA model. In this study, we selected ASCs that could be easily obtained from adipose

tissue among various MSC candidates, and isolated small EVs from hASCs using TFF multi-filtration system that enables scalable production and purification of sEVs for clinical use. We have demonstrated that the intra-articular injection of hASC-EVs could protect cartilage from degeneration and attenuate OA progression via the down-regulation of cartilage catabolic enzymes. In addition, we observed that both hASC-EVs and bone marrow mesenchymal stem cells-derived EVs (BM-MSC-EVs) have similar anti-inflammatory activity in IL-1 β -stimulated chondrocytes (Supplementary Figure S6). Although this study shows that hASC-EVs are effective in preventing OA progression, the mechanisms of their therapeutic effects on OA are not fully determined. Therefore, further detailed investigation of the internal contents and mechanism of action of hASC-EVs are necessary. Furthermore, the effective dose of EVs needs to be optimised in animal experiments.

In conclusion, we demonstrated that hASC-EVs effectively protect cartilage from degeneration and attenuate OA progression by modulating immune reactivity. Our findings showed that the hASC-EVs promoted the proliferation and migration of human OA chondrocytes, regulated the expression of catabolic and anticatabolic factors and suppressed macrophage infiltration into the synovium. Therefore, hASC-EVs should be considered a potential therapeutic approach in the treatment of OA.

Competing Interest

Yong Woo Cho and Dong-Gyu Jo are stockholders of Exostemtech Inc. Ji Suk Choi and Youn Jae Jung are employees of Exostemtech Inc. The other authors have no conflicts of interest to declare.

Contributors

C.H.W. performed experiments, processed the data and wrote the manuscript. Y.J.J., K.S.L. and W.S.K. contributed to EV isolation and characterisation. H.K.K., G.Y.J, J.H. and J.L. performed *in vivo* and *in vitro* experiments and analysed the data. Y.E.Y. performed *in vivo* experiments and processed the data. J.S.C. and J.H.P. contributed to the design of the study and discussed the results. D.G.J. designed the study, analysed the data and wrote the manuscript. Y.W. C. designed the study, financed the project and wrote the manuscript. D.G.J. and Y.W.C. contributed equally to the study and share correspondence.

Data sharing

All data are included in this manuscript and supplementary files.

Funding

This research was supported by the National Research Foundation (NRF) funded by the Korean Government (NRF-2018M3A9H1023767, NRF-2017R1A5A1070259, NRF-2019R1A5A2027340, NRF-2019R1A2C3011422), and a grant (18172MFDS173) from Ministry of Food and Drug Safety (MFDS).

References

- [1] Glyn-Jones S, Palmer AJR, Agricola R, et al. Osteoarthritis. *Lancet*. 2015;386:376–387.
- [2] Chen D, Shen J, Zhao W, et al. Osteoarthritis: toward a comprehensive understanding of pathological mechanism. *Bone Res*. 2017;5:16044.
- [3] Zhang W, Ouyang H, Dass CR, et al. Current research on pharmacologic and regenerative therapies for osteoarthritis. *Bone Res*. 2016;4:15040.
- [4] Gupta PK, Das AK, Chullikana A, et al. Mesenchymal stem cells for cartilage repair in osteoarthritis. *Stem Cell Res Ther*. 2012;3:25.
- [5] Caplan AI, Correa D. The msc: an injury drugstore. *Cell Stem Cell*. 2011;9:11–15.
- [6] Wu L, Leijten JC, Georgi N, et al. Trophic effects of mesenchymal stem cells increase chondrocyte proliferation and matrix formation. *Tissue Eng Part A*. 2011;17:1425–1436.
- [7] Yanez R, Lamana ML, Garcia-Castro J, et al. Adipose tissue-derived mesenchymal stem cells have in vivo immunosuppressive properties applicable for the control of the graft-versus-host disease. *Stem Cells*. 2006;24:2582–2591.
- [8] Ter Huurne M, Schelbergen R, Blattes R, et al. Antiinflammatory and chondroprotective effects of intra-articular injection of adipose-derived stem cells in experimental osteoarthritis. *Arthritis Rheum*. 2012;64:3604–3613.
- [9] Djouad F, Bouffi C, Ghannam S, et al. Mesenchymal stem cells: innovative therapeutic tools for rheumatic diseases. *Nat Rev Rheumatol*. 2009;5:392–399.
- [10] Lee WY, Wang B. Cartilage repair by mesenchymal stem cells: clinical trial update and perspectives. *J Orthop Translat*. 2017;9:76–88.
- [11] Jiang T, Xu G, Wang Q, et al. In vitro expansion impaired the stemness of early passage mesenchymal stem cells for treatment of cartilage defects. *Cell Death Dis*. 2017;8:e2851.
- [12] Xia Q, Zhu S, Wu Y, et al. Intra-articular transplantation of atsttrin-transduced mesenchymal stem cells ameliorate osteoarthritis development. *Stem Cells Transl Med*. 2015;4:523–531.
- [13] Lai RC, Yeo RW, Lim SK. Mesenchymal stem cell exosomes. *Semin Cell Dev Biol*. 2015;40:82–88.
- [14] Cosenza S, Ruiz M, Toupet K, et al. Mesenchymal stem cells derived exosomes and microparticles protect cartilage and bone from degradation in osteoarthritis. *Sci Rep*. 2017;7:16214.
- [15] Toh WS, Lai RC, Hui JHP, et al. Msc exosome as a cell-free msc therapy for cartilage regeneration: implications for osteoarthritis treatment. *Semin Cell Dev Biol*. 2017;67:56–64.
- [16] Kourembanas S. Exosomes: vehicles of intercellular signaling, biomarkers, and vectors of cell therapy. *Annu Rev Physiol*. 2015;77:13–27.
- [17] Phinney DG, Pittenger MF. Concise review: msc-derived exosomes for cell-free therapy. *Stem Cells*. 2017;35:851–858.
- [18] Tan CY, Lai RC, Wong W, et al. Mesenchymal stem cell-derived exosomes promote hepatic regeneration in drug-induced liver injury model. *Stem Cell Res Ther*. 2014;5:76–89.
- [19] Burrello J, Monticone S, Gai C, et al. Stem cell-derived extracellular vesicles and immune-modulation. *Front Cell Dev Biol*. 2016;4:83.
- [20] Zhao Y, Liu B, Liu CJ. Establishment of a surgically-induced model in mice to investigate the protective role of progranulin in osteoarthritis. *J Vis Exp*. 2014;84:e50924..
- [21] Moon SJ, Woo YJ, Jeong JH, et al. Rebamipide attenuates pain severity and cartilage degeneration in a rat model of osteoarthritis by downregulating oxidative damage and catabolic activity in chondrocytes. *Osteoarthritis Cartilage*. 2012;20:1426–1438.
- [22] Gimble JM, Katz AJ, Bunnell BA. Adipose-derived stem cells for regenerative medicine. *Circ Res*. 2007;100:1249–1260.
- [23] Fang B, Song Y, Zhao RC, et al. Using human adipose tissue-derived mesenchymal stem cells as salvage therapy for hepatic graft-versus-host disease resembling acute hepatitis. *Transplant Proc*. 2007;39:1710–1713.
- [24] Mazo M, Hernandez S, Gavira JJ, et al. Treatment of reperfused ischemia with adipose-derived stem cells in a preclinical swine model of myocardial infarction. *Cell Transplant*. 2012;21:2723–2733.
- [25] Baharlou R, Ahmadi-Vasmehjani A, Faraji F, et al. Human adipose tissue-derived mesenchymal stem cells in rheumatoid arthritis: regulatory effects on peripheral blood mononuclear cells activation. *Int Immunopharmacol*. 2017;47:59–69.
- [26] Lin G, Wang G, Liu G, et al. Treatment of type 1 diabetes with adipose tissue-derived stem cells expressing pancreatic duodenal homeobox 1. *Stem Cells Dev*. 2009;18:1399–1406.
- [27] Simonsen JB. Pitfalls associated with lipophilic fluorophore staining of extracellular vesicles for uptake studies. *J Extracell Vesicles*. 2019;8:1582237.
- [28] Chiou N-T, Ansel KM. Improved exosome isolation by sucrose gradient fractionation of ultracentrifuged crude exosome pellets. *Protoc Exch*. 2016. DOI:10.1038/protex.2016.057
- [29] Schmitz N, Laverty S, Kraus VB, et al. Basic methods in histopathology of joint tissues. *Osteoarthritis Cartilage*. 2010;18(Suppl 3):S113–6.
- [30] Thomas CM, Fuller CJ, Whittles CE, et al. Chondrocyte death by apoptosis is associated with cartilage matrix degradation. *Osteoarthritis Cartilage*. 2007;15:27–34.
- [31] Heard BJ, Solbak NM, Chung M, et al. The infrapatellar fat pad is affected by injury induced inflammation in the rabbit knee: use of dexamethasone to mitigate damage. *Inflamm Res*. 2016;65:459–470.
- [32] Glasson SS, Chambers MG, Van Den Berg WB, et al. The oarsi histopathology initiative - recommendations for

- histological assessments of osteoarthritis in the mouse. *Osteoarthritis Cartilage*. 2010;18(Suppl 3):S17–23.
- [33] Thery C, Witwer KW, Aikawa E, et al. Minimal information for studies of extracellular vesicles 2018 (misev2018): A position statement of the international society for extracellular vesicles and update of the misev2014 guidelines. *J Extracell Vesicles*. 2018;7:1535750.
- [34] Sellam J, Berenbaum F. The role of synovitis in pathophysiology and clinical symptoms of osteoarthritis. *Nat Rev Rheumatol*. 2010;6:625–635.
- [35] Valadi H, Ekstrom K, Bossios A, et al. Exosome-mediated transfer of mrnas and micrnas is a novel mechanism of genetic exchange between cells. *Nat Cell Biol*. 2007;9:654–659.
- [36] Akhtar N, Haqqi TM. MicroRNA-199a* regulates the expression of cyclooxygenase-2 in human chondrocytes. *Ann Rheum Dis*. 2012;71:1073–1080.
- [37] Matsukawa T, Sakai T, Yonezawa T, et al. MicroRNA-125b regulates the expression of aggrecanase-1 (adamts-4) in human osteoarthritic chondrocytes. *Arthritis Res Ther*. 2013;15:1–11.
- [38] Xu J, Liu Y, Deng M, et al. MicroRNA221-3p modulates ets-1 expression in synovial fibroblasts from patients with osteoarthritis of temporomandibular joint. *Osteoarthritis Cartilage*. 2016;24:2003–2011.
- [39] Mao G, Zhang Z, Huang Z, et al. MicroRNA-92a-3p regulates the expression of cartilage-specific genes by directly targeting histone deacetylase 2 in chondrogenesis and degradation. *Osteoarthritis Cartilage*. 2017;25:521–532.
- [40] Zhang S, Chu WC, Lai RC, et al. Exosomes derived from human embryonic mesenchymal stem cells promote osteochondral regeneration. *Osteoarthritis Cartilage*. 2016;24:2135–2140.
- [41] Tao SC, Yuan T, Zhang YL, et al. Exosomes derived from mir-140-5p-overexpressing human synovial mesenchymal stem cells enhance cartilage tissue regeneration and prevent osteoarthritis of the knee in a rat model. *Theranostics*. 2017;7:180–195.
- [42] Akkiraju H, Nohe A. Role of chondrocytes in cartilage formation, progression of osteoarthritis and cartilage regeneration. *J Dev Biol*. 2015;3:177–192.
- [43] Favero M, Ramonda R, Goldring MB, et al. Early knee osteoarthritis. *RMD Open*. 2015;1:e000062.
- [44] Goldring MB, Otero M, Tsuchimochi K, et al. Defining the roles of inflammatory and anabolic cytokines in cartilage metabolism. *Ann Rheum Dis*. 2008;67(Suppl 3):iii75–82.
- [45] Kapoor M, Martel-Pelletier J, Lajeunesse D, et al. Role of proinflammatory cytokines in the pathophysiology of osteoarthritis. *Nat Rev Rheumatol*. 2011;7:33–42.
- [46] Malfait AM, Liu RQ, Ijiri K, et al. Inhibition of adam-ts4 and adam-ts5 prevents aggrecan degradation in osteoarthritic cartilage. *J Biol Chem*. 2002;277:22201–22208.
- [47] Mengshol JA, Vincenti MP, Coon CI, et al. Interleukin-1 induction of collagenase 3 (matrix metalloproteinase 13) gene expression in chondrocytes requires p38, c-jun n-terminal kinase, and nuclear factor kappaB: differential regulation of collagenase 1 and collagenase 3. *Arthritis Rheum*. 2000;43:801–811.
- [48] Daheshia M, Yao JQ. The interleukin 1 β pathway in the pathogenesis of osteoarthritis. *J Rheumatol*. 2008;35:2306.
- [49] Glasson SS, Askew R, Sheppard B, et al. Deletion of active adamts5 prevents cartilage degradation in a murine model of osteoarthritis. *Nature*. 2005;434:644–648.
- [50] Echtermeyer F, Bertrand J, Dreier R, et al. Syndecan-4 regulates adamts-5 activation and cartilage breakdown in osteoarthritis. *Nat Med*. 2009;15:1072–1076.
- [51] Manfredini C, Maumus M, Gabusi E, et al. Adipose-derived mesenchymal stem cells exert antiinflammatory effects on chondrocytes and synoviocytes from osteoarthritis patients through prostaglandin e2. *Arthritis Rheum*. 2013;65:1271–1281.
- [52] Desando G, Cavallo C, Sartoni F, et al. Intra-articular delivery of adipose derived stromal cells attenuates osteoarthritis progression in an experimental rabbit model. *Arthritis Res Ther*. 2013;15:R22.
- [53] Platas J, Guillen MI, Del Caz MD, et al. Conditioned media from adipose-tissue-derived mesenchymal stem cells downregulate degradative mediators induced by interleukin-1beta in osteoarthritic chondrocytes. *Mediators Inflamm*. 2013;2013:357014.
- [54] Pers YM, Quentin J, Feirreira R, et al. Injection of adipose-derived stromal cells in the knee of patients with severe osteoarthritis has a systemic effect and promotes an anti-inflammatory phenotype of circulating immune cells. *Theranostics*. 2018;8:5519–5528.
- [55] Tofino-Vian M, Guillen MI, Del Caz MDP, et al. Microvesicles from human adipose tissue-derived mesenchymal stem cells as a new protective strategy in osteoarthritic chondrocytes. *Cell Physiol Biochem*. 2018;47:11–25.
- [56] Visse R, Nagase H. Matrix metalloproteinases and tissue inhibitors of metalloproteinases: structure, function, and biochemistry. *Circ Res*. 2003;92:827–839.
- [57] Chadjichristos C, Ghayor C, Kypriotou M, et al. Sp1 and sp3 transcription factors mediate interleukin-1 beta down-regulation of human type ii collagen gene expression in articular chondrocytes. *J Biol Chem*. 2003;278:39762–39772.
- [58] Dumond H, Presle N, Pottie P, et al. Site specific changes in gene expression and cartilage metabolism during early experimental osteoarthritis. *Osteoarthritis Cartilage*. 2004;12:284–295.
- [59] Drexler SK, Kong PL, Wales J, et al. Cell signalling in macrophages, the principal innate immune effector cells of rheumatoid arthritis. *Arthritis Res Ther*. 2008;10:216–227.
- [60] Fahy N, de Vries-van Melle ML, Lehmann J, et al. Human osteoarthritic synovium impacts chondrogenic differentiation of mesenchymal stem cells via macrophage polarisation state. *Osteoarthritis Cartilage*. 2014;22:1167–1175.